ISSN 1330-3651 (Print), ISSN 1848-6339 (Online) https://doi.org/10.17559/TV-20230628000770
Original scientific paper

The Modern Single Shaft Gas Turbine Rotor Stress-Strain State Determination Taking into Account the Contact Thermoelasticity Problem

Natalia SMETANKINA, Serhii MORHUN*

Abstract: The paper outlines a finite elements refined mathematical model of the stress-strain state of single shaft gas turbine engine that can be used in ground or floating power plants. The mathematical model, built on the basis of special contact finite elements takes into consideration the contact thermoelasticity problem in the joint area of disk and blades. On the basis of the developed mathematical model the fields of turbine rotor dynamic stresses and displacement have been found too. To make the clear decision about the developed mathematical model adequacy mostly loaded impeller dynamic stresses field has been found and verified by comparison with the calculated results without contact and experimental data. The divergence between the calculated data and experimental results is less than 8%. The turbine rotor displacements and dynamic stresses have been found for different forced vibration modes for the wide range of harmonic indexes changing from 0 to 4. The obtained results along with the previous studies of this rotor fluid flow and thermal state could be used in further studies of the turbine rotor creep and fatigue strength and blades crack researches.

Keywords: contact thermoelasticity problem; dynamic stresses field; experimental verification; finite elements method; gas turbine rotor

1 INTRODUCTION

In modern conditions of gas turbine engines construction development, it is extremely necessary to increase the engine's capacity, durability and reliability. To ensure the required level of reliability of the developed gas turbine engines, we need to solve a number of problems in different areas, such as fluid flow dynamics, heat transfer, mechanics of solid deformable body etc. On the other hand, all of these problems are interconnected, because the results of one problem solution are used as initial data for the other problems solution. Thus for the purpose of the modern single shaft three stages turbine rotor stress-strain state study the results of the fluid flow and thermal state analysis for this rotor are used as initial data [1, 2]. In the working process of gas turbine rotors, which are used in modern turbines, various mechanical and thermal loads of high intensity are constantly present. All these factors seriously influence the rotor impellers stress-strain state. For their stress-strain state determination it is absolutely important to take into account the thermal and mechanical conditions in the impellers contact area. Also the basic contact conditions of the impellers are not always the same [1]. In the vast majority of papers each impeller and even the whole rotor is considered as one monolith solid body but this assumption does not fully correspond to the real working conditions. This means that each pair of contact surfaces has its own specific pairing conditions. But during the workflow, pairing conditions can change quickly. This fact causes changes in the nature of mechanical contact. Therefore, we can also observe changes in the heat flow parameters on the contact surfaces inside each impeller and between the impellers [2]. Therefore, the mathematical model used to solve the problem of thermoelasticity of gas turbine engine rotors must take into account all these mechanical and temperature changes on the contact surfaces of the parts forming the rotor. There are two main approaches that are used to solve contact problems of solid mechanics by the finite element method (FEM). The main idea of the first approach is to use a contact layer with a certain thermal conductivity, which is located between the surfaces of the blades and disk, forming the impeller [3]. The finite element model of the contact layer is based on finite elements similar to those of impeller's parts [3]. But it should also be mentioned that it is extremely difficult to calculate the deformation of the layer caused by the thermal gradient on the contacting surfaces. The second main approach is to use a layer of special contact elements that clearly defines the relationship between the heat flux and the displacements of the finite element nodes located on the contact surfaces [3-6]. But there are several important requirements. The first is the condition of non-penetration of the contacting parts into each other; the second is the condition of equality of the normal and tangential force components for each pair of nodes of contacting finite elements [4-9]. In paper [5] the authors have studied the thermal stress-strain state of the turbine blades, but did not take into consideration the contact problems. In paper [6] special attention has been paid to the problems of solid continuum meshing, but yet the problems of the turbine blades vibration have not been studied. In papers [7-9] the thermo-mechanical problems have been considered, but there is a lack of attention to the issues of the thermo-mechanical contact between the blades and disk. The issues of the whole rotor stress-strain state are studied slightly too. Based on the analysis of the above sources, it can be concluded that at the moment there are still a number of unsolved problems regarding the design of highly loaded single shaft marine GTE rotors through numerical methods. One of them is the turbine rotor stress-strain state determination taking into consideration contact thermoelasticity problem. This study would be held on the basis of FEM, using the layer of special contact finite elements.

2 THE AIM AND OBJECTIVES OF STUDY

The research object is the turbine rotor stress-strain state taking into consideration the contact between the blades and disks. The whole rotor should be considered as an assembly of three impellers, connected together. Each impeller also is an assembly that consists of the disk and working blades of the same shape and geometric characteristics. The research subject is the influence of contact in the joint of rotor blades and disks on its fields of dynamic stresses. Thus the aim of the research is to develop

a refined mathematical model for calculating the gas turbine rotor stress-strain state taking into account the rotor contact thermoelasticity problem solution. To achieve this aim, the following tasks must be solved:

- Develop a refined mathematical model of the turbine rotor on the basis of FEM, using the layer of contact finite elements between the blades and disks surfaces.
- Determine the contact finite elements displacement and temperature fields.
- Determine the field of rotor dynamic stresses, taking into account the results of contact thermoelasticity problem solution.

3 FORMULATION OF THE PROBLEM

The rotor of the gas turbine engine under study is located in the right rectangular Cartesian coordinate system XYZ with the center at point O. The X axis is normal to the turbine rotor axis of rotation of the shaft; the Z axis coincides with this axis (Fig. 1). The entire coordinate system rotates at a constant angular velocity Ω together with the rotor.

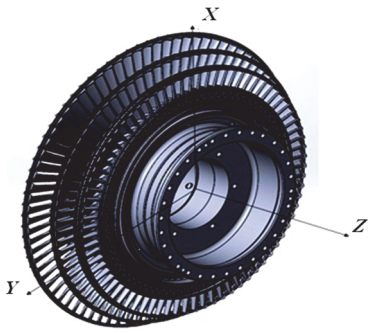

Figure 1 Gas turbine rotor in the Cartesian right-handed coordinate system

3.1 Main Dependences for the Rotor Stress-strain State Study

According to the generalized Hooke's law [3, 10, 11] the solid body stress-strain state can be described by the next matrix dependence:

$$\{\sigma\} = [D](\{\varepsilon\} - \{\varepsilon_T\}) \tag{1}$$

where $\{\sigma\}$ is stress matrix-vector; $\{\mathcal{E}\}$ is elasticity deformation vector; $\{\mathcal{E}_T\}$ is thermal elasticity vector; $[D]$ is elasticity matrix of the turbine rotor material. As the turbine rotor is located in Cartesian coordinate system, its elasticity deformation vector has the following components:

$$\{\varepsilon\} = \begin{Bmatrix} \varepsilon_X \\ \varepsilon_Y \\ \varepsilon_Z \\ \gamma_{XY} \\ \gamma_{XZ} \\ \gamma_{YZ} \end{Bmatrix} = \begin{Bmatrix} \frac{\partial \delta_X}{\partial X} \\ \frac{\partial \delta_Y}{\partial Y} \\ \frac{\partial \delta_Z}{\partial Z} \\ \frac{\partial \delta_X}{\partial Y} + \frac{\partial \delta_Y}{\partial X} \\ \frac{\partial \delta_X}{\partial Z} + \frac{\partial \delta_Z}{\partial X} \\ \frac{\partial \delta_Y}{\partial Z} + \frac{\partial \delta_Z}{\partial Y} \end{Bmatrix} \tag{2}$$

where δ_X, δ_Y, δ_Z are components of the generalized displacement vector. The rotor material is a special nickel-titanium alloy. The vector of the rotor thermal deformation is represented by the Eq. (3) [8, 11-14]:

$$\{\varepsilon_T\} = \begin{Bmatrix} \varepsilon_{XT} \\ \varepsilon_{YT} \\ \varepsilon_{ZT} \\ 0 \\ 0 \\ 0 \end{Bmatrix} = \alpha \begin{Bmatrix} T_X \\ T_Y \\ T_Z \end{Bmatrix} \tag{3}$$

where α is thermal extension coefficient of the rotor material; T_X, T_Y, T_Z are the rotor temperature field projections on the X, Y, Z coordinate axis. Thus on the basis of Eq. (1) to Eq. (3) we see that solution to the turbine rotor stress-strain state problem depends on the correct finding of the rotor displacement and temperature fields, taking into account the contact between the blades and disks in impellers.

4 SOLUTION TO THE PROBLEM AND ITS VERIFICATION

4.1 Mechanical Contact Problem

The energy state of the impeller's contact area can be described using the Lagrange variation principle in the following way:

$$\begin{aligned} &\delta L = 0 \\ &L = \Pi - W \end{aligned} \tag{4}$$

where L is Lagrange function; Π is the rotor contact deformation potential energy; W is the contact forces work. Between the contacting surfaces of blades and disk we need to insert a layer of special two nodes contact elements (EL2) (Fig. 2). The whole impellers are approximated by the eight nodes hexagonal finite elements (EL8) [3, 15, 16].

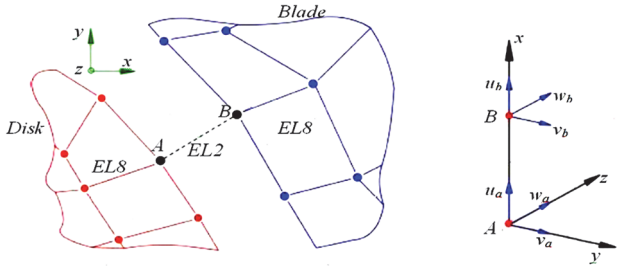

Figure 2 Scheme of the contact between the disk and blade in impeller and the special contact element EL2: *u, v, w*-displacement of the contact finite element

So, after the FEM approximation the potential energy of the finite element contact deformation can be formed as follows [12, 19]:

$$\begin{aligned} &\Pi_e = \frac{1}{2}\iiint_{V_e} \{\varepsilon_e\}^T [D]\{\varepsilon_e\}\,dV = \\ &= \frac{1}{2}\iiint_{V_e} \{\delta_e\}^T [B_e]^T [D][B_e]\{\delta_e\}\,dV \\ &e = 1, ..., m \end{aligned} \tag{5}$$

where $[B_e]$ contact finite element gradient matrix; $\{\delta_e\}$ contact finite element displacement vector; V_e finite element volume; m number of the contact elements EL2.

$$[B_e]=\begin{bmatrix} \frac{\partial N_i}{\partial x_i} & 0 & 0 \\ 0 & \frac{\partial N_i}{\partial y_i} & 0 \\ 0 & 0 & \frac{\partial N_i}{\partial z_i} \end{bmatrix} \quad (6)$$
$$i=1,\ 2$$

where $[N]$ finite contact element shape functions matrix; i number of finite contact element nodes. The contact forces work [17]:

$$W_e=\{\delta_e\}^T\{F_e\} \quad (7)$$
$$e=1,\ ...,\ m$$

where $\{F_e\}$ vector of the finite element contact forces. Substituting Eq. (5) and Eq. (6) into Eq. (4) and differentiating by displacement we receive:

$$L=\Sigma_{e=1}^{m}\left(1/2\int_{V_e}\{\delta_e\}^T[B_e]^T[D][B_e]\{\delta_e\}\,\mathrm{d}V - \right.$$
$$\left.-\{\delta_e\}^T[F_e]\right) \quad (8)$$
$$\frac{\partial L}{\partial\{\delta\}}=\Sigma_{e=1}^{m}\left(\frac{1}{2}\int_{V_e}[B_e]^T[D][B_e]\{\delta_e\}\,\mathrm{d}V-[F_e]\right)=0$$
$$e=1,\ ...,\ m$$

As it has been known from [1, 3, 5, 18]: $[K_e]=\int_{V_e}[B_e]^T[D][B_e]\{\delta_e\}\,\mathrm{d}V$, where $[K_e]$ the finite element stiffness matrix. The vector of contact forces for the contact element AB (Fig. 2) is formed as follows:

$$\{F_e\}=\begin{bmatrix} p_\eta & 0 & 0 \\ 0 & p_\tau & 0 \\ 0 & 0 & p_\tau \end{bmatrix}\{\delta_{AB}\} \quad (9)$$

where p_n and p_τ are normal and tangential components of contact pressure, that are formed by the mounting tightness in the process of impeller parts conjugation; $\{\delta_{AB}\}$ is vector of the contact element displacement discrepancy. $\{\delta_{AB}\}=\begin{Bmatrix} x_B-x_A \\ y_B-y_A \\ z_B-z_A \end{Bmatrix}$. Thus on the basis of dependences Eq. (4) to Eq. (9) the mechanical contact problem for the turbine rotor is represented by the next matrix equation:

$$[K_e]\{\delta_e\}=\{F_e\} \quad (10)$$
$$e=1,\ ...,\ m$$

It also should be mentioned that the contact elements obey the law of non-penetration for the contacting surfaces.

4.2 Thermal Contact Problem

The thermal state of the impeller's contact area can be described by the next functional:

$$\delta J_K=0 \quad (11)$$

where J_K is thermal functional. The subsequence of such thermal functional minimization and its FEM approximation are given in paper [11]. Thus we obtain:

$$\frac{\partial J_K}{\partial\{T\}}=\Sigma_{e=1}^{m}[\Lambda_{KTe}]\{T_{Ke}\}+[Q_{Ke}] \quad (12)$$
$$e=1,\ ...,\ m$$

where $[\Lambda_{KTe}]$ is matrix of the contact finite element thermal conductivity; $\{T_{Ke}\}$ is vector of the contact element temperature; $\{Q_{Ke}\}$ is intensity of the heat flow passing through the contact elements. The intensity of contact heat flow is given by the next dependence:

$$[Q_{Ke}]=\begin{bmatrix} \lambda_K & 0 & 0 \\ 0 & \lambda_K & 0 \\ 0 & 0 & \lambda_K \end{bmatrix}\{T_{AB}\} \quad (13)$$
$$e=1,\ ...,\ m$$

where λ_k is contact thermal conductivity.

$$\lambda_k=\frac{\lambda T_{AB}}{l_{AB}};\ T_{AB}=T_B-T_A \quad (14)$$

where λ is the impeller material thermal conductivity; l_{AB} is length of the contact finite element; T_{AB} is contact element temperature discrepancy. Thus on the basis of dependences Eq. (11) to Eq. (14) the thermal contact problem for the turbine rotor is represented by the next matrix equation:

$$[\Lambda_{Ke}]\{T_{Ke}\}=\{Q_{Ke}\} \quad (15)$$
$$e=1,\ ...,\ m$$

Using the matrix dependencies Eq. (10) and Eq. (15) we can find the fields of displacement and temperature on contact surfaces of rotor disks and blades. These data is needed to use the dependencies Eq. (1) to Eq. (3) and thus to solve the turbine rotor contact thermoelasticity problem. After solving this problem we use the obtained data and the data given in papers [2, 18, 19] to determine the refined stress-strain state of the whole turbine rotor.

4.3 Verification of the Developed Mathematical Model

For the verification of the developed mathematical model an experimental investigation has been held. On the surface of the most hardly loaded first impeller the special sensors have been mounted. The digital data from sensors have been transmitted to a special decoder and compared with the calculated results. The experiment has been carried out with a steady air flow that corresponds with the real conditions of the turbine rotor working process as a

part of a GTE. The description of experimental equipment and experiment order are given in papers [12, 17]. The results of the maximum dynamic stresses definition for experimental and both numerical types (taking and without taking into consideration the contact problem) are given in Tab. 1 and Tab. 2.

Table 1 The first impeller maximum dynamic stresses without taking into account the contact problem

Harmonic index k	Maximum dynamic stresses σ / MPa		Divergence / %
	Calculated data	Experimental data	
0	431.71	419.9	2.6
1	481.96	455.9	5.4
2	528.34	489.8	7.3
3	650.18	596.8	8.2
4	769.26	708.5	7.9

Table 2 The first impeller maximum dynamic stresses taking into account the contact problem

Harmonic index k	Maximum dynamic stresses σ / MPa		Divergence / %
	Calculated data	Experimental data	
0	426.20	419.9	1.53
1	473.12	455.9	3.77
2	502.83	489.8	2.66
3	628.39	596.8	5.29
4	754.12	708.5	6.04

Analyzing the data, represented in Tab. 1 and Tab. 2, we can conclude that the divergence between the calculated results and experimental data is less than 10%. But it also should be highlighted that the value of the dynamic stresses in Tab. 2 is lower as well as closer to experimental data. Thus the developed mathematical model which takes into account the mechanical and thermal contact problems in the blades and disk joint is more adequate and accurate due to the less divergence with the experimental data. So its usage is more preferable.

5 RESULTS AND DISCUSSION

The power of the turbine under study P is 15 MW. The temperature of the working fluid at the flow path entrance T is 1410 K; the total pressure at the first stage entrance p is 1.4 MPa; the rotor angular velocity ω is 11330 rev/min. As it was shown in Tab. 1 and Tab. 2 the turbine rotor dynamic stresses increase with the increase of the rotor forced vibration frequency. So, we need to show correctly the fields of rotor displacements / mm and stresses / MPa. for the first four harmonic indexes. These results for both components are given in Fig. 3 to Fig. 6.

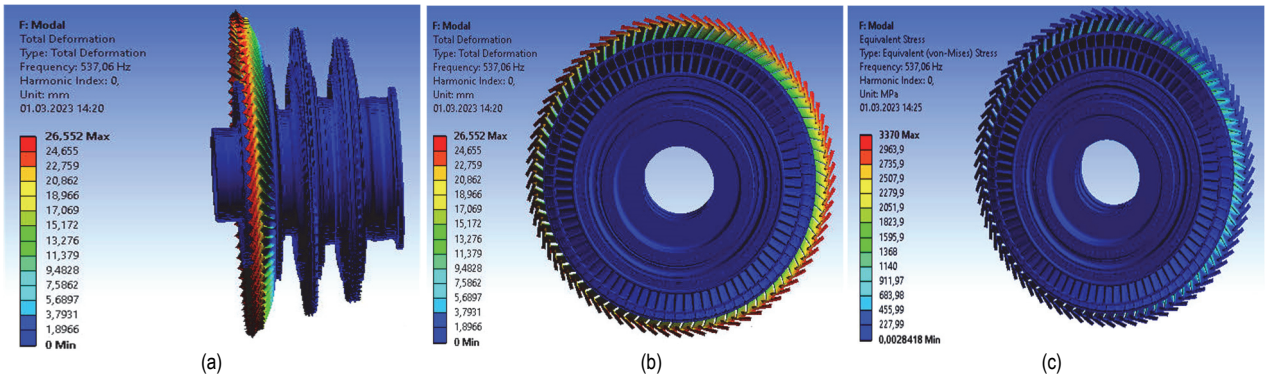

(a) (b) (c)

Figure 3 Turbine rotor displacement (a, b) and dynamic stresses (c) fields. Harmonic index k = 0, vibration frequency f = 537.06 Hz

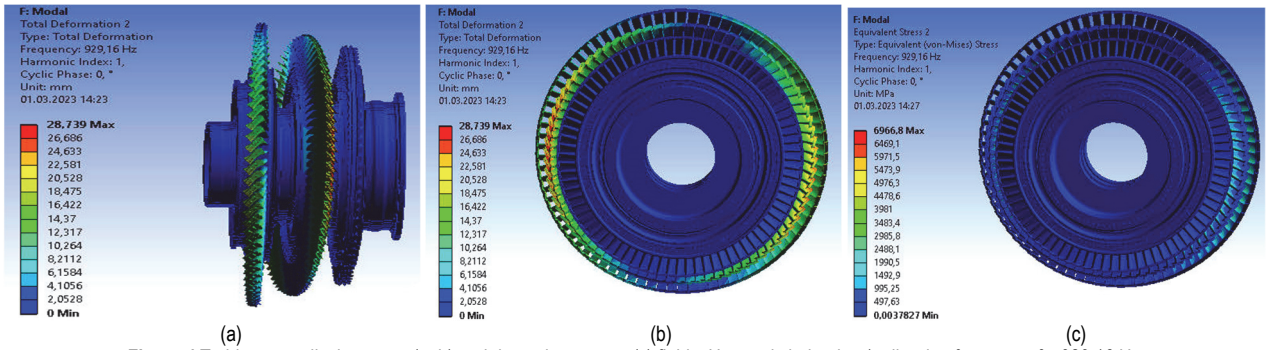

(a) (b) (c)

Figure 4 Turbine rotor displacement (a, b) and dynamic stresses (c) fields. Harmonic index k = 1, vibration frequency f = 929.16 Hz

Analyzing data represented in Fig. 3 to Fig. 6 we can see that with the increase of the turbine rotor vibration frequency the level of its dynamic stresses increases too. The biggest displacement in these directions is nearly 50 mm on the top of the third impeller blades peripheral section for the vibration frequency of 1040 Hz. It can be explained by the influence of gas flow and centrifugal force. The third impeller blades according to their geometric characteristics are more malleable than the first impeller blades. Dynamic stresses, caused by the complex influence of gas flow and centrifugal force, increase with the increase of the rotor vibration frequency. The gap between the highest stresses for harmonic index 0 and harmonic index 3 is nearly 400 MPa. Furthermore, the drop of dynamic stresses is present even between the different parts of the blade, because the gas flow influences more blade feather peripheral part and it is hot up more than the blade root part. We also need to take into consideration that the level of the rotor maximum dynamic stresses for the vibration mode with the harmonic index k = 3 nearly reaches the rotor ultimate strength.

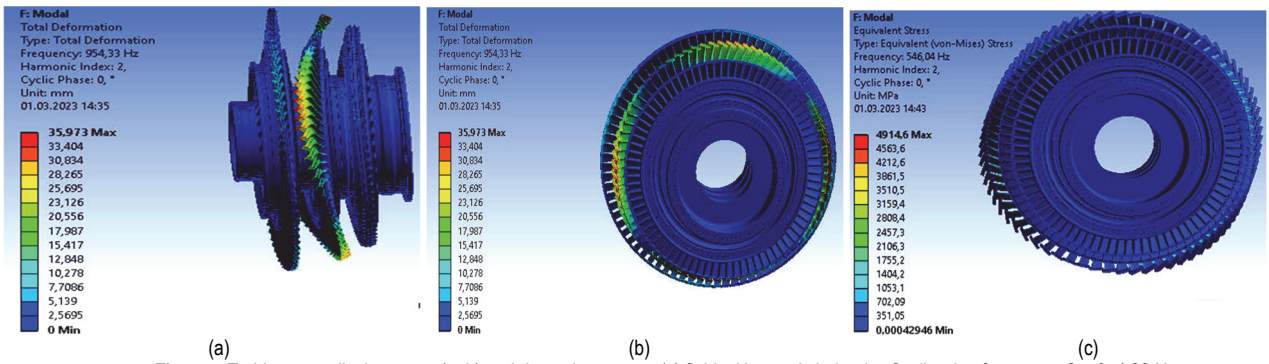

(a) (b) (c)

Figure 5 Turbine rotor displacement (a, b) and dynamic stresses (c) fields. Harmonic index k = 2, vibration frequency Ω = 954.33 Hz

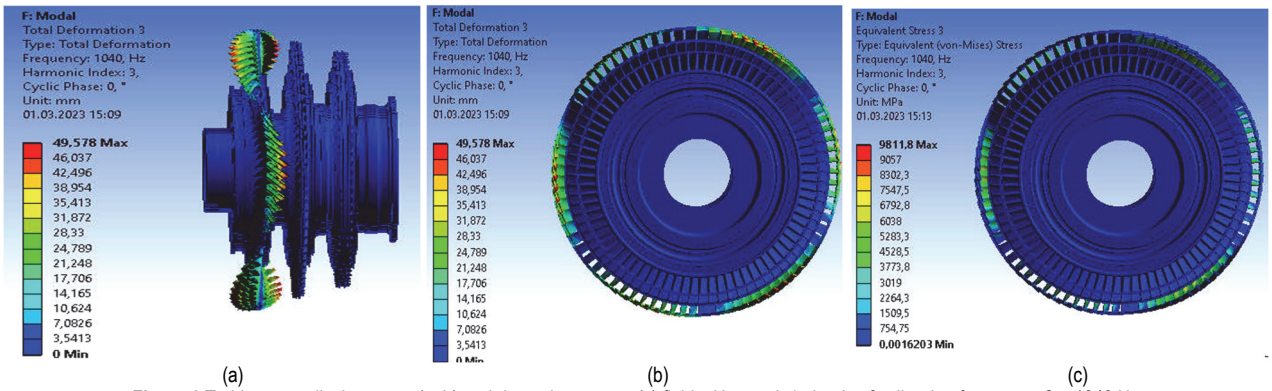

(a) (b) (c)

Figure 6 Turbine rotor displacement (a, b) and dynamic stresses (c) fields. Harmonic index k = 3, vibration frequency Ω = 1040 Hz

6 CONCLUSIONS

The study of the modern single shaft gas turbine rotor stress-strain state has been held. To solve the aforementioned problem a refined mathematical model based on the solving of contact thermoelasticity problem in the joint area of blades and disk was developed. The reliability and adequacy of this mathematical model are confirmed by comparison with the calculation data (without contact problem) and experimental data. Using the developed mathematical model, the rotor fields of displacement and dynamic stresses have been studied too. It has been shown that the increase of the rotor forced vibration frequency causes the increases of the rotor dynamic stresses level. Such stresses are caused by the influence of gas flow and centrifugal forces. The sharp temperature gradient between the peripheral part of the blade, its root part and the disk is also one of the main reasons for such gap in dynamic stresses for different part of the blade and disk. The big temperatures of the gas flow [2] and the dynamic stresses level are the reasons for the new studies in the fields of the turbine rotor plasticity and creep. All the obtained results together with the data given in [1, 2] and methodology given in [20] would be used for further studies of the modern GTE rotor creep and fatigue strength. The findings of the work are applicable in the areas of the power plants engine building, aircraft and marine engine building too.

7 REFERENCES

[1] Morhun, S. & Vilkul, S. (2022). Gas dynamic analysis of the modern single shaft gas turbine engine flow path. *International Journal of Turbo and Jet Engines*. https://doi.org/10.1515/tjeng-2022-0019

Morhun, S. (2022). Numerical analysis of the gas turbine rotor blades thermal state using a refined mathematical model. *Lecture Notes in Networks and Systems*, *344*, 115-123. https://doi.org/10.1007/978-3-030-89902-8_9

[2] Zienkiewicz, O. C. (2014). *The Finite Element Method for Solid and Structural Mechanics*. Elsevier/Butterworth-Heinemann, Amsterdam, Boston.

[3] Mzarbhuiya, H. M. S. M. & Pandey, K. M. (2017). Steady state structural analysis of high pressure gas turbine blade using finite element analysis. *IOP Conf. Series: Material Science and Engineering*. https://doi.org/10.1088/1757-899X/225/1/012113

[4] Ziaei-Asl, A. & Tayefe-Ramezanlou, M. (2019). Thermo-mechanical behavior of gas turbine blade equipped with cooling ducts and protective coating with different thickness. *International Journal of Mechanical Sciences*, *150*, 656-664. https://doi.org/10.1016/j.ijmecsci.2018.10.070

[5] Yershov, S. V. & Yakovlev, V. A. (2021). The influence of mesh resolution on 3D RANS flow simulations in turbomachinery flow path. *Journal of Mechanical* Engineering, *24*(1), 13-27. https://doi.org/10.15407/pmach2021.01.013

[6] Aniekan, I. E., Oghenefeijro, E. O. E., & Godfrey, A. O. (2018). Thermo-structural analysis of first stage gas turbine rotor blade materials for optimum service performance. *International Journal of Engineering and Applied Sciences*, *10*(2), 118-130. https://doi.org/10.24107/ijeas.447650

[7] Kumar, R., Kumar, V. S., Butt, M. M., Sheikh, N. A., Khan, S. A., & Afzal, A. (2020). Thermo-mechanical analysis and estimation of turbine blade tip clearance of a small gas turbine engine under transient operating conditions. *Applied Thermal Engineering*. https://doi.org/10.1016/j.applthermaleng.2020.115700

[8] Liu, W. (2016). Design and kinetic analysis of wind turbine blade-hub-tower coupled system. *Renewable energy*, *94*, 547-557. https://doi.org/10.1016/j.renene.2016.03.068

[9] Eliseev, V. & Moskalets, A. (2016). Application of the Lagrange-Ritz-Kantorovich method to the vibration analysis of turbine blades. *NTU "KhPI" Bulletin: Power and heat*

engineering processes and equipment, *8*, 149-152. https://doi.org/10.20998/2078-774X.2016.08.21
[10] Boychenko, N. & Ishtyryakov, I. (2019). Characterization of the stress-strain state in a gas turbine engine compressor disk taking into account damage accumulation. *Frattura ed IntegritaStruturalle*, *50*, 54-67. https://doi.org/10.3221/IGF-ESIS.50.07
[11] Duriagina, Z. A., Kulyk, V. V., Filimonov, O. S., Trostianchyn, A. M., & Sokulska, N. B. (2021).The role of stress-strain state of gas turbine engine metal parts in predicting their safe life. *Progress in Physics of Metals*, *22*(4), 643.677. https://doi.org/10.15407/ufm.22.04.643
[12] Bitkina, O., Weon-Kang, K., & Jang-Ho, L. (2015). Experimental and theoretical analysis of the stress-strain state of anisotropic multilayer composite panels for wind turbine blade. *Renewable Energy*, *79*, 219-226. https://doi.org/10.1016/j.renene.2014.11.004
[13] Skamniottis, Ch., Courtis, M., & Cocks, C. F. A. (2021). Multiscale analysis of thermomechanical stresses in double wall transpiration cooling systems for gas turbine blades. *International Journal of Mechanical Sciences.* https://doi.org/10.1016/j.ijmecsci.2021.106657
[14] Kauss, O., Tsybenko, H., Naumenko, K., Hutter, S., & Kruger, M. (2019).Structural analysis of gas turbine blades made of Mo-Si-B under transient thermo-mechanical loads. *Composite Materials Sciences*, *165,* 129.136. https://doi.org/10.1016/j.commatsci.2019.04.023
[15] Narasimbachary, S. B., Smith, K., Schinde, R. S., Amann, C., Kadau, K., & Iyer, S. (2019). Life assessment of large turbine blades. *ASME Turbo Expo 2019: Turbomachinery Technical Conference and Exposition Proceeding Paper.* https://doi.org/10.1115/GT2019-91630
[16] Arkhipov, A. N., Volgina, M. V., Matushkin, A. A., Ravikovich, Y. A., & Kholobtsev, D. P. (2018). Effect of a model and boundary conditions on the results of analyzing the stress-strain state of a low pressure compressor rotor. *Structural Mechanics and Strength of Flight Vehicles*, *61,* 509-516. https://doi.org/10.3103/S1068799818040025
[17] Kantor, B. Y., Smetankina, N. V., & Shupikov, A. N. (2001). Analysis of non-stationary temperature fields in laminated strips and plates. *International Journal of Solids and Structures*, *38*(48/49), 8673-8684. https://doi.org/10.1016/S0020-7683(01)00099-3
[18] Misura, S., Smetankina, N., & Misiura, I. (2021). Optimal design of the cyclically symmetrical structure under static load. *Integrated Computer Technologies in Mechanical Engineering - 2020. ICTM 2020. Lecture Notes in Networks and Systems*, *188*, 256-266. https://doi.org/10.1007/978-3-030-66717-7_21
[19] Cazin, D., Braut, S., & Zigulic R. (2009). Fatigue life analysis of the damaged steam turbine blade. *Engineering Review*, *29*(2), 33-43.

Contact information:

Natalia SMETANKINA, PhD, Professor
Department of Vibration and Thermostability Studies, Anatolii Pidhornyi Institute of Mechanical Engineering Problems of the National Academy of Sciences of Ukraine,
2/4 Dmytra Pozharskogo Street, Kharkiv, Ukraine
E-mail: n.smetankina@ukr.net

Serhii MORHUN, PhD, Associate Professor
(Corresponding author)
Department of Engineering Mechanics and Technology of Machinebuilding, Admiral Makarov National University of Shipbuilding,
9 Heroiv Ukrainy Avenue, Mykolaiv, Ukraine
E-mail: serhii.morhun@nuos.edu.ua